Available online at www.sciencedirect.com
SCIENCE DIRECT
Journal of Catalysis 236 (2005) 313–323
JOURNAL OF CATALYSIS
www.elsevier.com/locate/jcat

Zirconia-supported heteropoly acids: Characterization and catalytic behavior in liquid-phase veratrole benzoylation

Biju M. Devassy, S.B. Halligudi *

Inorganic Chemistry and Catalysis Division, National Chemical Laboratory, Pune - 411 008, India

Received 28 April 2005; revised 8 September 2005; accepted 13 September 2005

Available online 10 November 2005

Abstract

The liquid-phase benzoylation of veratrole with benzoic anhydride (BA) to 3,4-dimethoxy benzophenone was investigated using zirconia-supported silicotungstic acid (STA) as a catalyst. Catalysts with different STA loadings (5–25 wt%) and calcination temperatures (600–850 °C) were prepared by suspending zirconium oxyhydroxide in methanol solution of STA followed by drying and calcination. These catalysts were characterized by XRD, Raman spectroscopy, DTA, XPS, NH_3-TPD, FTIR pyridine adsorption, and DRUV–vis spectroscopy. XRD results indicated that the presence of STA retarded the crystallization of zirconia and stabilized ZrO_2 in tetragonal phase. Characterization of the catalyst with optimum STA loading (15%) by Raman spectroscopy showed the presence of zirconia-anchored mono-oxotungstate as the major tungsten species up to 750 °C. The catalysts showed both Brönsted and Lewis acidity, and 15% STA on zirconia calcined at 750 °C (15 SZ-750) had the highest Brönsted acidity and total acidity. The catalytic activity was found to depend on STA coverage, and the highest activity corresponded to the monolayer of silicotungstate on zirconia. Further, a comparison of the catalytic activity of 15 SZ-750 with zirconia-supported phosphotungstic acid (15%, calcined at 750 °C, 15 PZ-750) and silica-supported silicotungstic acid (15%, calcined at 300 °C, 15 SS-300) showed that silicotungstic acid and phosphotungstic acid supported on zirconia acted as efficient and stable solid acid catalysts, whereas silicotungstic acid supported on silica was leached into the reaction medium and catalyzed the reaction homogeneously. Under the reaction conditions of 120 °C and a veratrole-to-BA molar ratio of 5, the most active catalyst, 15 SZ-750, showed 99% BA conversion, and the deactivated catalyst could be regenerated by calcination without appreciable loss in activity.

Keywords: Zirconia; Silicotungstic acid; Phosphotungstic acid; Benzoylation; Veratrole

1. Introduction

Friedel–Crafts acylation reactions are of great importance in the industrial manufacture of aryl ketones and also are used extensively in the production of pharmaceuticals, insecticides, dyes, and other commercial products. Conventionally, these reactions are carried out in presence of aluminium chloride, using an acylating agent, such as acid chloride, in a volatile organic solvent [1]. Because of the complexation of the product ketone with aluminum chloride, stoichiometric excess of the catalyst must be used, which is then destroyed in the hydrolysis step required for product isolation. The large quantities of metal salt waste formed, as well as the production of HCl, have aroused much research interest in the development of new, cleaner technologies that generate minimal waste. A major step toward waste minimization would be to develop a truly catalytic process, using an acid anhydride, where the catalyst does not form a strong complex with product and is recyclable. At present, considerable efforts are being made to find efficient, sustainable, recyclable, and eco-friendly solid acid catalysts to serve as substitutes for current homogeneous Brönsted and Lewis acids. Various catalysts, including zeolites [2–5], heteropoly acids (HPAs) [6–9], and sulfated metal oxides [10–12], have been tested for this reaction.

HPAs are a unique class of materials active in both redox and acid catalysis [13–15]. These are polyoxometallates composed of heteropoly anions with metal–oxygen octahedra as the basic structural unit. The Keggin-type HPAs are the most important in

* Corresponding author.
E-mail addresses: sb.halligudi@ncl.res.in, halligudi@cata.ncl.res.in (S.B. Halligudi).

0021-9517/$ – see front matter
doi:10.1016/j.jcat.2005.09.016

catalysis, and 12-tungstophosphoric acid (phosphotungstic acid [PTA]) and 12-tungstosilicic acid (silicotungstic acid [STA]) are the usual catalysts of choice because of their high acidic strength, relatively high thermal stability, and lower oxidation potential compared with molybdenum HPAs. These are strong Brönsted acid catalysts, with a strength of acidity greater than that of conventional solid acids such as zeolites and mixed oxides [14].

HPAs can be used either directly as a bulk material or in supported form. The supported form is preferable because of its higher surface area compared with the bulk material (5–8 $m^2\,g^{-1}$) and better accessibility of reactants to the active sites. Acidic or neutral solids, which interact weakly with HPAs such as silica, active carbon, and acidic ion-exchange resin, have been reported to be suitable HPA supports [16]. A serious problem associated with these types of materials is their susceptibility to deactivation during organic reactions due to the formation of carbonaceous deposit (coke) on the catalyst surface. The thermal stability of HPAs is not sufficiently high to carry out conventional regeneration by burning coke at 500–550 °C, as is routinely used for zeolites and aluminosilicates [17]. HPAs are highly soluble in polar solvents and hence can leach from the catalyst surface to the reaction medium and catalyze the reaction homogeneously. Thus the preparation of HPA in supported form, which is active and stable at high temperature and in the presence of polar reactants, is essential to fully realize the potential of these materials as catalysts.

In recent years, zirconia has attracted much attention as both a catalyst and a catalyst support because of its high thermal stability and the amphoteric character of its surface hydroxyl groups [18,19]. Zirconia modified with anions like sulfate and tungstate act as strong solid acid catalysts [20,21]. In attempts to find suitable supports for HPAs, zirconia was found to be promising [22–24]. Recently, we have shown that zirconia can be used as an efficient support for HPAs [25–27].

The present study deals with the preparation of zirconia-supported silicotungstic acid and its characterization by XRD, Raman spectroscopy, DTA, XPS, NH_3-TPD, FTIR pyridine adsorption, and DRUV–vis spectroscopy. These catalysts were used in benzoylation of veratrole (1,2-dimethoxy benzene) with benzoic anhydride, and the activity of the most active catalyst 15 SZ-750 was compared with that of 15 PZ-750 and 15 SS-300.

2. Experimental

2.1. Materials

Zirconyl chloride ($ZrOCl_2 \cdot 8H_2O$) and ammonia (25%) were obtained from S.D. Fine Chemicals, Ltd., Mumbai. Veratrole (98%), 12-STA ($H_4SiW_{12}O_{40} \cdot nH_2O$), 12-PTA ($H_3PW_{12}O_{40} \cdot nH_2O$), tetraethyl orthosilicate (TEOS, $Si(OC_2H_5)_4$), and methanol were purchased from Aldrich. Benzoic anhydride (98%) was obtained from E. Merck India, Ltd., Mumbai. All chemicals were used as received without further purification.

2.2. Catalyst preparation

The catalysts were prepared by suspending a known amount of dried zirconium oxyhydroxide powder in a methanol solution of STA. Zirconium oxyhydroxide was prepared by hydrolysis of 0.5 M of zirconyl chloride solution by the dropwise addition of aqueous NH_3 (10 M) to a final pH of 10. The precipitate was filtered and washed with ammoniac water (pH = 8) until it was free from chloride ions as determined by the silver nitrate test. The zirconium oxyhydroxide thus obtained was dried at 120 °C for 12 h, powdered well, and dried for another 12 h. Each time, 4 ml of methanol per g of solid support was used, and the mixture was stirred in a rotary evaporator for 8–10 h. After stirring, the excess of methanol was removed at ca. 50 °C under vacuum. The resulting solid materials were dried at 120 °C for 24 h and ground well. A series of catalysts with different STA loadings (5–25%) were prepared by varying the STA concentration in methanol. The dried samples were then calcined in air. All samples were calcined in shallow quartz boats placed inside a 3-cm-diameter quartz tube in a tube furnace. The samples were heated at a rate of 5 °C min^{-1} to the final temperature and held for 4 h under static conditions, then cooled at a rate of 5 °C min^{-1} to room temperature. For comparison, catalysts with 15% PTA on zirconia (calcined at 750 °C; 15 PZ-750) and 15% STA on silica gel (calcined at 300 °C; 15 SS-300) were also prepared [28]. The support silica gel was prepared by the hydrolysis of TEOS in presence of HNO_3 followed by drying at 120 °C for 12 h, powdering, and further drying for another 12 h. The catalysts with STA on ZrO_2 are represented by xSZ-T, where x represents wt%, S represents STA, Z represents zirconia, and T denotes calcination temperature (°C).

2.3. Characterization

The specific surface areas of the catalysts were measured by N_2 physisorption at liquid nitrogen temperature using a Quantachrome Nova-1200 surface area analyzer and standard multipoint BET analysis methods. Samples were degassed in flowing N_2 for 2 h at 300 °C before N_2 physisorption measurements.

X-Ray diffraction (XRD) measurements of the catalyst powder were recorded using a Rigaku Geigerflex diffractometer equipped with Ni-filtered Cu-K_α radiation ($\lambda = 1.5418$ Å).

Raman spectra of the catalyst 15 SZ calcined at different temperatures were recorded on powder samples at room temperature with a Bruker IFS 66 spectrometer connected to a Raman module FRA 106. The 1.06-μm line of the NdYAG laser was used for excitation, and the spectral resolution was 3 cm^{-1}.

The ^{31}P MAS NMR spectrum of the catalyst 15 PZ-750 was recorded using a Bruker DSX-300 spectrometer at 121.5 MHz with high-power decoupling with a Bruker 4-mm probe head. The spinning rate was 10 KHz, and the delay between two pulses was varied between 1 and 30 s to ensure complete relaxation of the ^{31}P nuclei. The chemical shifts are given relative to external 85% H_3PO_4.

Differential thermal analysis (DTA) measurements were performed on a Pyris Diamond TG-DTA apparatus from room temperature to 1000 °C in flowing dry oxygen (ca. 50 ml min^{-1}),

using α-Al_2O_3 as a reference. For each experiment, 5–8 mg of the sample was used, with a heating rate of 20 °C min^{-1}.

X-Ray photoelectron spectroscopy (XPS) measurements were performed on a VG Microtech Multilab ESCA 3000 spectrometer with a nonmonochromatized Mg-K_α X-ray source. Energy resolution of the spectrometer was set at 0.8 eV with Mg-K_α radiation at a pass energy of 50 eV. The binding energy correction was performed using the C1s peak of carbon at 284.9 eV as a reference.

The acidity of the catalysts were measured by temperature-programmed desorption of NH_3 (NH_3-TPD) using a Micromeritics AutoChem-2910 instrument. It was carried out after ~0.5 g of the catalyst sample was dehydrated at 600 °C in He (30 cm^3 min^{-1}) for 1 h. The temperature was decreased to 100 °C, and NH_3 was adsorbed by exposing samples treated in this manner to a stream containing 10% NH_3 in He for 1 h at 100 °C. It was then flushed with He for another 1 h to remove physisorbed NH_3. The desorption of NH_3 was carried out in He flow (30 cm^3 min^{-1}) by increasing the temperature to 600 °C at a rate of 10 °C min^{-1} and measuring NH_3 desorption using a TCD detector.

The nature of the acid sites (Brönsted and Lewis) of the catalyst samples were characterized by in situ Fourier transform infrared (FTIR) spectroscopy with chemisorbed pyridine. The pyridine adsorption studies were carried out in the diffuse reflectance infrared Fourier transform (DRIFT) mode using a Shimadzu SSU 8000 instrument. A calcined powder sample in a sample holder was placed in a specially designed cell. The samples were then heated in situ from room temperature to 400 °C at a heating rate of 5 °C min^{-1} in a flowing stream (40 ml min^{-1}) of pure N_2. The samples were kept at 400 °C for 3 h, then cooled to 100 °C; then pyridine vapor (20 µl) was introduced under N_2 flow, and the IR spectra were recorded at different temperatures up to 400 °C. A resolution of 4 cm^{-1} was attained after averaging over 500 scans for all of the IR spectra reported here.

Diffuse reflectance UV–vis (DRUV–vis) spectra of catalyst samples were obtained using a Shimadzu UV-2101 PC spectrometer equipped with a diffuse–reflectance attachment, with $BaSO_4$ as the reference. The reflectance spectra were converted into the Kubelka–Munk function, ($F(R)$), which is proportional to the absorption coefficient for low values of $F(R)$.

2.4. Catalyst testing

The liquid-phase benzoylation reactions were carried out in a 50-ml glass batch reactor (slurry reactor) with an anhydrous $CaCl_2$ guard tube. The reaction temperature was maintained by a silicon oil bath equipped with a thermostat and magnetic stirrer. The catalyst freshly activated at 500 °C for 2 h was weighed in the reactor, and then veratrole was added according to the proportion desired. Finally benzoic anhydride was added to obtain the desired molar ratio of veratrole to benzoic anhydride. A typical reaction mixture consisted of 3.77 g (27.2 mmol) of veratrole, 1.23 g of benzoic anhydride (5.4 mmol), and 0.15 g of catalyst. After 1 h, the reaction was stopped and the catalyst separated. The filtrate was analyzed using a Shimadzu 14B gas chromatograph with an HP-5 capillary column (cross-linked 5% ME silicone, 30 m × 0.53 × 1.5 µm film thickness), coupled with FID. The product identification was carried out using GC-MS and by comparing with authentic standards.

Table 1
Surface area, surface density and acidity of various catalysts

Catalyst	Surface area (m^2 g^{-1})	Surface density (W nm^{-2})	Acidity[a] (NH_3 nm^{-2})
Z-750	16	0	ne[b]
5 SZ-750	43	3.1	2.63
10 SZ-750	50	5.4	2.77
15 SZ-750	55	7.4	2.81
20 SZ- 750	54	10	2.71
25 SZ-750	52	13.1	2.65
15 SZ-600	125	3.2	ne
15 SZ-650	108	3.7	1.93
15 SZ-700	80	5.0	2.43
15 SZ-800	46	8.7	2.61
15 SZ-850	36	11.4	ne
15 PZ-750	53	7.2	3.29

[a] Acidity values obtained from NH_3-TPD.
[b] Not evaluated.

3. Results and discussion

3.1. Characterization of the catalysts

3.1.1. Surface area

The pure zirconium oxyhydroxide dried at 120 °C showed a surface area of 332 m^2 g^{-1}; after calcination at 750 °C, the surface area decreased to 16 m^2 g^{-1}. Adding STA to the support resulted in an increased surface area, reaching a maximum at 15% STA loading (Table 1). This was due to the strong interaction of STA with the support, which reduces the surface diffusion of zirconia and inhibits sintering and stabilizes the tetragonal phase of zirconia, leading to an increase in surface area. Above 15% STA loading, surface area did not change appreciably, possibly due to the formation of crystalline WO_3, which likely narrowed or plugged the pores of the samples.

The nominal WO_3 loading corresponding to each STA loading and calcination temperature was determined to calculate the tungsten (W) surface density using the measured surface area. The tungsten surface densities, expressed as the number of W atoms per nanometer square area (W atoms nm^{-2}), were obtained by the equation

$$\text{W surface density} = \{[\text{WO}_3 \text{ loading (wt\%)}/100] \times 6.023 \times 10^{23}\} / [231.8 \text{ (formula weight of WO}_3) \times \text{BET surface area } (m^2\,g^{-1}) \times 10^{18}]$$

and are presented in Table 1. The values show that an increase of the STA loading resulted in an increased W surface density. The specific surface area of SZ catalyst also depends on the calcination temperature. The W surface density increased with the calcination temperature because of the concominant decrease in the ZrO_2 surface area (Table 1).

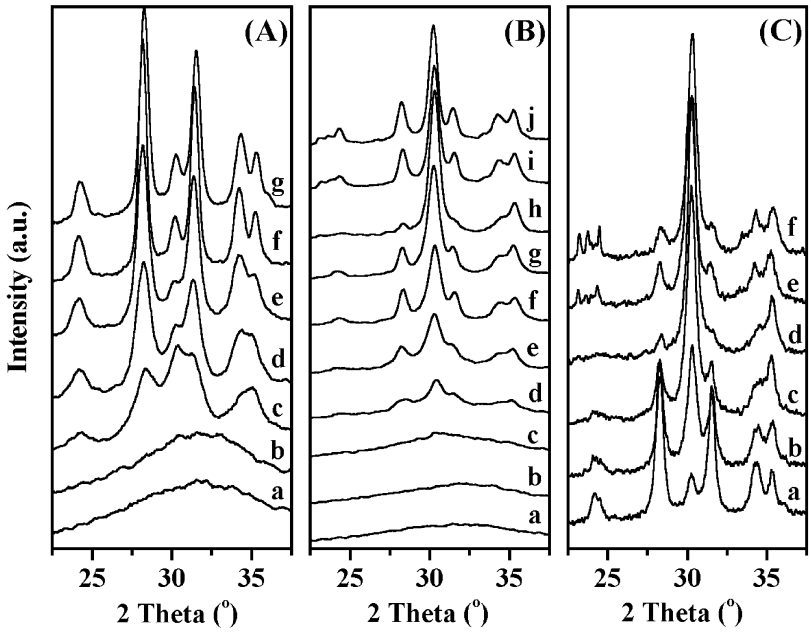

Fig. 1. X-Ray diffractograms of (A) ZrO_2 calcined at (a) 120, (b) 250, (c) 350, (d) 450, (e) 550, (f) 650, (g) 750 °C, (B) 15 SZ calcined at different temperatures (a) 120, (b) 250, (c) 350, (d) 450, (e) 550, (f) 650, (g) 700, (h) 750, (i) 800, (j) 850 °C, and (C) catalysts with different STA loading calcined at 750 °C (a) 0, (b) 5, (c) 10, (d) 15, (e) 20, (f) 25%.

3.1.2. X-Ray diffraction

The bulk structure of pure ZrO_2 and of supported HPA catalysts were determined by powder X-ray diffraction (Fig. 1). The support showed amorphous behavior below 350 °C and crystallized to a mixture of monoclinic and tetragonal phases, and the intensity of monoclinic phase increased with increasing calcination temperature. The XRD patterns of the catalysts with different STA loadings calcined at 750 °C show that the presence of STA strongly influenced the crystallization of zirconium oxyhydroxide into zirconia. Pure zirconia calcined at 750 °C is mainly monoclinic, with only a small amount of the tetragonal phase. For catalysts with low STA loading calcined at 750 °C, the XRD pattern can be described as the sum of the monoclinic and tetragonal phases of zirconia, with this latter phase becoming dominant for catalysts with 15% STA.

As shown in Fig. 1, 15% catalyst was amorphous when calcined below 450 °C, and as the calcination temperature increased, zirconia crystallized progressively to tetragonal phase. At 750 °C, the catalyst existed mainly in the tetragonal phase, and above 750 °C, formation of monoclinic phase of zirconia was observed. The effectiveness of the surface species in stabilizing ZrO_2 in the tetragonal phase may be lost at high temperatures, because they diffuse into the bulk, decompose, and desorb, or "dewet" and agglomerate to form poorly interacting clusters as a separate phase [29]. Thus the added STA stabilizes the tetragonal phase of zirconia, and we have noted such stabilization of tetragonal ZrO_2 in the presence of HPAs [25,26]. In addition, at up to a 15% STA loading for catalysts calcined at 750 °C and for 15% catalysts up to 750 °C calcination, no diffraction lines attributed to the polyacid or its decomposition products were observed, indicating that STA is highly dispersed on the support. With an STA loading > 15%, or a calcination temperature > 750 °C for 15% loading, new diffraction lines appeared in the 23–25° region, characteristic of WO_3 [30].

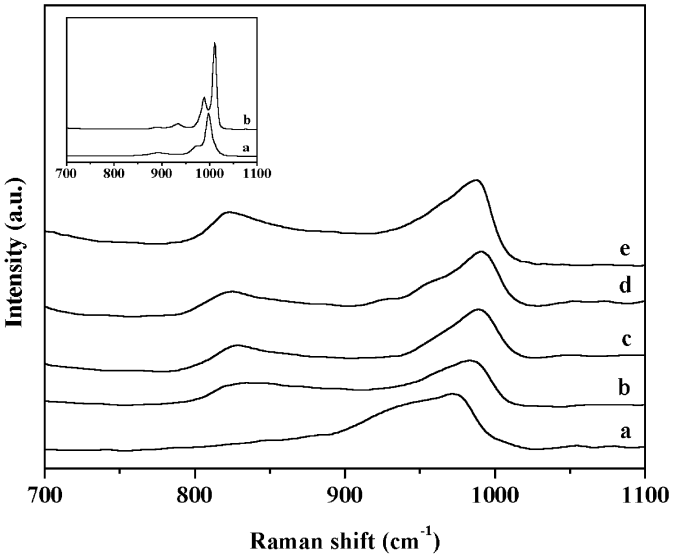

Fig. 2. Raman spectra of the catalysts (a) 15 SZ-120, (b) 15 SZ-650, (c) 15 SZ-700, (d) 15 SZ-750, (e) 15 PZ-750. Inset: (a) STA, (b) PTA.

3.1.3. Raman spectroscopy and ^{31}P MAS NMR spectroscopy

Raman spectra of pure STA and the catalyst 15 SZ calcined at different temperatures are shown in Fig. 2. The strong support Raman bands below 700 cm^{-1} interfered with the diagnostic Raman bands of tungstate species, whereas the range above 700 cm^{-1} was free from characteristic bands of ZrO_2 and hence was relevant to the structure determination of tungsten species. Pure STA showed a sharp band at 998 cm^{-1} with a distinct shoulder at 974 cm^{-1}. The bands at 998 and 974 cm^{-1} can

be attributed to $\nu_{(W=O)}$ symmetric and asymmetric stretching modes. In addition, another broad band observed at 893 cm^{-1} can be assigned to the $\nu_{(W–O–W)}$ asymmetric stretching mode [31,32]. Pure PTA showed a similar Raman spectrum as that of pure STA. The catalyst 15 SZ-120 showed a broad band with two components at 973 and at 946 cm^{-1}. These bands appeared to be red-shifted in comparison with pure STA, which could be due to the partial weakening of W=O bonds, possibly due to the interaction of STA with the support [23]. The position of $\nu_{(W=O)}$ band was shifted from 973 to 992 cm^{-1} with an increase in calcination temperature from 120 to 750 °C, indicating an increase in W=O bond order. The increase in $\nu_{(W=O)}$ wave number with calcination temperature could be due to an increase in the agglomeration of silicotungstate species [33]. This is also evidenced by the increase in tungsten surface density with calcination temperature (Table 1). At a calcination temperature of 650 °C and above, Raman spectra showed a new band centered near 825 cm^{-1}. Scheithauer et al. assigned this band to the $\nu_{(W–O–W)}$ stretching mode [34]. Recently, Loridant et al. proved that this band originates from $\nu_{(W–O–Zr)}$ vibration and not from $\nu_{(W–O–W)}$ vibration [33]. In addition to the bands at 825 and 992 cm^{-1}, the catalyst 15 SZ-750 showed an additional band at 910 cm^{-1} due to the $\nu_{(W–O–W)}$ stretching mode [4]. However, the relative intensity of this band was very small in comparison with other bands, indicating the formation of small amount of polyoxotungstate species [21,34]. Raman spectra of the catalyst 15 SZ did not show bands at 720 and 807 cm^{-1} characteristic of WO_3 up to a calcination temperature of 750 °C. The catalyst 15 PZ-750 showed bands at 988 and 822 cm^{-1} due to $\nu_{(W=O)}$ and $\nu_{(W–O–Zr)}$ vibrations, respectively.

The ^{31}P MAS NMR and ^{31}P CP/MAS NMR spectra of the catalyst 15 PZ-750 are shown in Fig. 3. The NMR spectra show signals above and below −20 ppm. The CP/MAS NMR spectrum indicates the attenuation of the signal above −20 ppm, and hence this signal is attributed to the P–OH group associated with phosphotungstate, which is in interaction with zirconia [25,26], whereas the signal below −20 ppm is attributed to phosphorous oxide resulting from the decomposition of phosphotungstic acid [23]. Elemental analysis by inductively coupled plasma-optical emission spectroscopy (ICP-OES) showed the composition of the catalyst 15 PZ-750 to be Zr = 62.22 wt%, W = 10.13 wt%, and P = 0.15 wt%, indicating that the P:W atomic ratio is ∼1:12. This result indicates that the phosphorous oxide formed by the decomposition of phosphotungstic acid was not lost by sublimation during calcination.

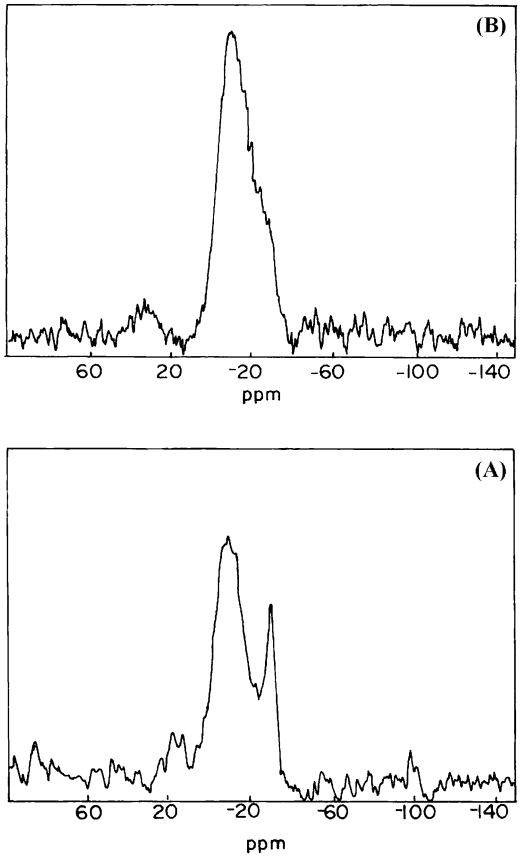

Fig. 3. ^{31}P MAS NMR spectrum (A) and ^{31}P CP/MAS NMR spectrum (B) of the catalyst 15 PZ-750.

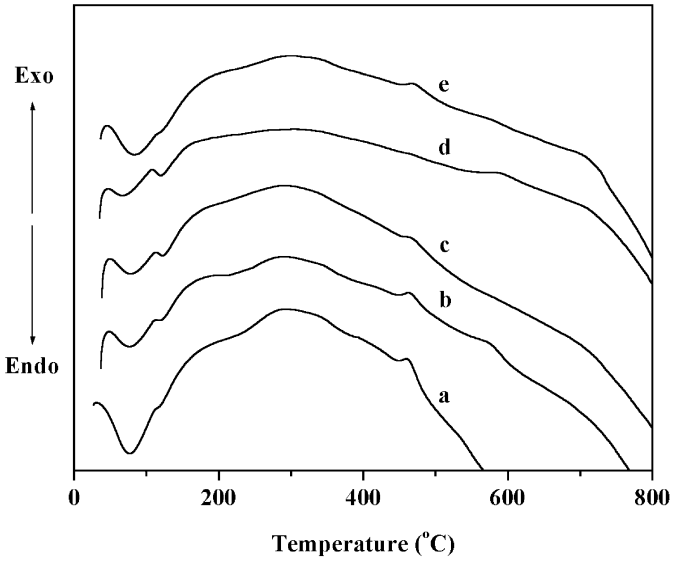

Fig. 4. DTA curves of catalysts with different STA loading dried at 120 °C (a) 5, (b) 10, (c) 15, (d) 20, (e) 25%.

3.1.4. Differential thermal analysis (DTA)

The catalysts with different STA loadings dried at 120 °C were characterized by differential thermal analysis (Fig. 4). The DTA of pure STA and zirconium oxyhydroxide (not shown) showed exothermic peaks at 548 and 452 °C, due to the decomposition of silicotungstic acid to its constituent oxides [35] and the crystallization of zirconium oxyhydroxide to zirconia. The catalyst 5 SZ showed an exothermic peak at 459 °C, whereas the other catalysts showed an additional exothermic peak shifted slightly from 573 °C for the catalyst 10 SZ to 595 °C for the catalyst 20 SZ. The catalyst 25 SZ exhibited a broad exothermic effect in the temperature range 690–738 °C, which could be due to the crystallization of WO_3.

Valigi et al. [36] showed that zirconium oxyhydroxide is microporous (< 2 nm diameter) in nature and consists of aggregates of primary particles that stick together to form large

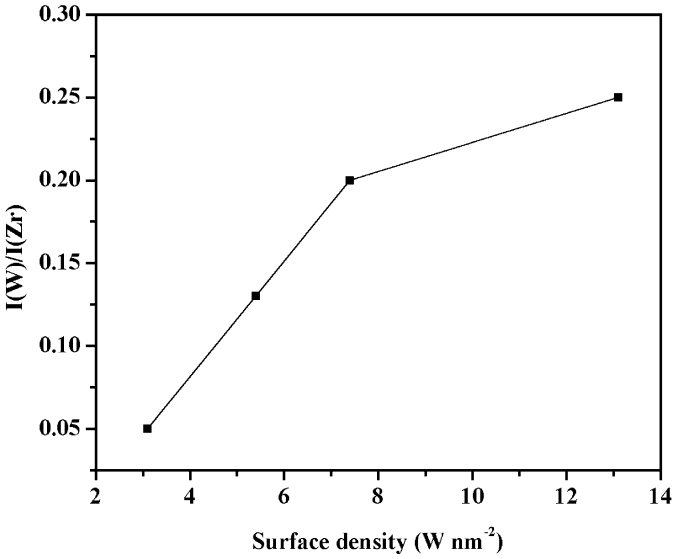

Fig. 5. Change in XPS intensity ratio $I(W)/I(Zr)$ with tungsten surface density.

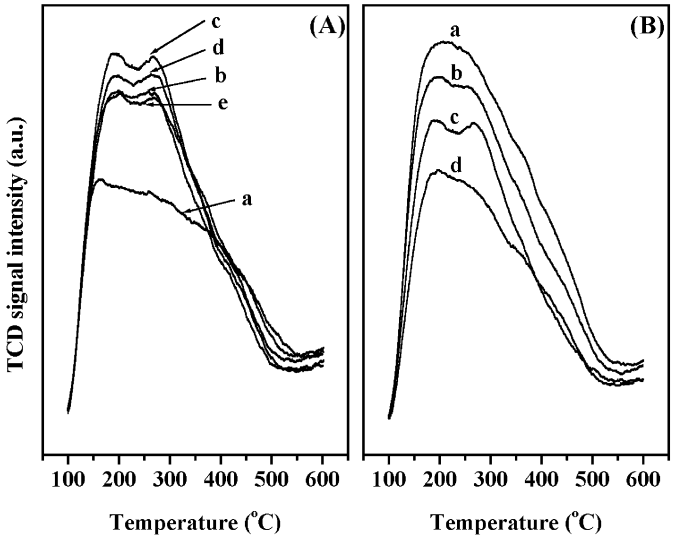

Fig. 6. NH_3-TPD profile of (A) catalyst with different STA loading calcined at 750 °C (a) 5, (b) 10, (c) 15, (d) 20, (e) 25% and (B) 15 SZ calcined at different temperatures (a) 650, (b) 700, (c) 750, (d) 800 °C.

grains. When the microporous zirconium oxyhydroxide is in contact with a solution of STA, the polyoxoanions can adsorb on the external surface of the grains and diffuse into the pores together with the solvent molecules. As the micropores fill with the solvent, the driving force for diffusion is the concentration gradient along the pores. Because the size of the Keggin anion (12 Å) is on the order of the pore size of the support, the rate of diffusion is controlled by the anion size, and thus larger polyoxoanions should have a lower diffusion rate. As a result, the large polyanions fail to reach all of the internal surfaces of zirconium oxyhydroxide.

When the samples are heated in oxidizing atmosphere, the support undergoes dehydration, causing surface shrinkage, and then crystallizes, whereas the adsorbed species can decompose or can interact with the support and form anchored species. The unsupported zirconia crystallizes through an exothermic effect at around 460 °C, whereas zirconia interacting with STA appears at higher temperatures.

3.1.5. X-Ray photoelectron spectroscopy

The XPS spectra of the catalysts with different tungsten surface densities showed an almost constant $W4f_{7/2}$ binding energy of 36 eV, which is characteristic of W(VI). The variation of the $I(W4f)/I(Zr3d)$ intensity ratio with tungsten surface density ($W\,nm^{-2}$) is used for estimating the monolayer coverage of STA on ZrO_2 [37,38]. The $I(W4f)/I(Zr3d)$ intensity ratio increased linearly with surface density up to 7.4 $W\,nm^{-2}$ (catalyst 15 SZ-750) and deviated from linearity with further increases in surface density (Fig. 5). This suggests that the deposition of the tungstate species is not uniform with increasing tungsten surface density and that deviation from linearity occurs at near-monolayer coverage. Furthermore, the theoretical surface coverage of STA on zirconia is calculated using the average surface area occupied per Keggin ion (144 $Å^2$) [39] and the nominal $H_4SiW_{12}O_{40}$ loading on ZrO_2 (calculated from the weight loss obtained in TG analysis) [29] and is found to be ~90%, which is close to the monolayer coverage of STA on zirconia.

3.1.6. TPD of NH_3

The ammonia adsorption–desorption technique usually enables determination of the strength of acid sites present on the catalyst surface together with total acidity. The NH_3-TPD profiles of the catalysts with different STA loadings and of the 15 SZ catalysts calcined at different temperatures are shown in Fig. 6, and the amounts of NH_3 desorbed per nm^2 are presented in Table 1. All samples showed a broad TPD profile, revealing that the surface acid strength was widely distributed. It is evident from Table 1 that there was an initial increase in the acidity until 15% loading, after which it decreased with further loading. For 15 SZ catalysts calcined at different temperatures, the amount of desorbed ammonia increased with calcination temperature and reached a maximum at 750 °C.

3.1.7. FTIR pyridine adsorption

Adsorption of pyridine as a base on the surface of solid acids is one of the most frequently applied methods for the characterization of surface acidity. The use of IR spectroscopy to detect adsorbed pyridine allows one to distinguish among different acid sites. The FTIR pyridine adsorption spectra of catalysts with different STA loadings calcined at 750 °C and 15 SZ catalysts calcined at different temperatures are shown in Fig. 7. The spectra showed sharp pyridine absorption bands at 1604, 1485, 1444, 1636, and 1534 cm^{-1}. Pyridine molecules bonded to Lewis acid sites absorbed at 1604 and 1444 cm^{-1}, whereas those responsible for Brönsted acid sites (pyridinium ion) showed absorbance at 1534 and 1636 cm^{-1} [40]. The band at 1485 cm^{-1} is a combined band originating from pyridine bonded to both Brönsted and Lewis acid sites.

The intensity of Brönsted (B) and Lewis (L) acid sites, obtained from the absorbance at 1534 and 1444 cm^{-1} [41], and the corresponding B/L ratios calculated, are shown in Fig. 8. At

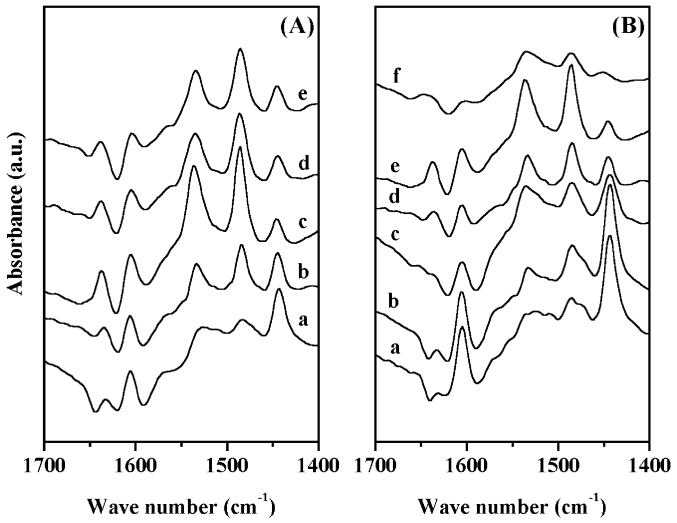

Fig. 7. FTIR pyridine adsorption spectra of (A) catalyst with different STA loading calcined at 750 °C (a) 5, (b) 10, (c) 15, (d) 20, (e) 25% and (B) 15 SZ calcined at different temperatures (a) 450, (b) 550, (c) 650, (d) 700, (e) 750, (f) 800 °C after in situ activation at 300 °C.

low loading, the catalyst showed mainly Lewis acidity; with an increase in loading Lewis acidity decreased, whereas Brönsted acidity increased and reached a maximum at 15% STA loading. An increase in STA loading above 15% decreased the Brönsted acidity, but with Lewis acidity remaining similar to that of 15% catalyst. The decrease in acidity above 15% could be due to the formation of crystalline WO_3, which prevents the accessibility of pyridine to the active sites. As in the case of catalysts with different loadings, the nature of acidity also depends on calcination temperature. At low calcination temperature (450 °C), the catalyst 15 SZ showed mainly Lewis acidity with very low Brönsted acidity that increases with calcination temperature up to 750 °C. Thus the Brönsted acidity of the catalyst increased

Table 2
Pyridine adsorption data for the catalysts 15 SZ-750 and 15 PZ-750 at different activation temperatures[a]

Activation temperature (°C)	B acidity I(B)	L acidity I(L)	B/L ratio I(B)/I(L)
100	0.19(0.15)	0.14(0.17)	1.36(0.88)
200	0.16(0.16)	0.09(0.12)	1.78(1.33)
300	0.10(0.09)	0.04(0.06)	2.50(1.5)
400	0.05(0.08)	0 (0.03)	ne[b] (2.67)

[a] For the catalyst 15 PZ-750, B, L and B/L values are indicated in parentheses.
[b] Not evaluated.

with both loading and calcination temperature up to a monolayer of STA on ZrO_2.

The IR absorbance intensities of Brönsted and Lewis acid sites of the catalysts 15 SZ-750 and 15 PZ-750 and the corresponding B/L ratio at different activation temperatures are given in Table 2. The results indicate that an increase of activation temperature resulted in a decrease in both Brönsted and Lewis acidity but an overall increase in Brönsted character (B/L ratio) of the catalyst. These results clearly show that the strength of the Brönsted acid sites was higher than that of the Lewis acid sites. Moreover, the catalyst 15 SZ-750 showed higher Brönsted acidity, whereas 15 PZ-750 showed higher Lewis acidity under all activation temperatures.

3.1.8. *Diffuse–reflectance UV–vis spectroscopy*

Diffuse–reflectance UV–vis spectra of pure STA, 15 SZ-750, and Z-750 are shown in Fig. 9. The pure STA bands observed in the range of 3–5.5 eV arose from a low-energy O^{2-} to W^{6+} charge transfer. The energy of an electronic transition can be characterized by the position of the energy of maximum absorption [42]. Because the charge-transfer bands were broad for the zirconia-supported STA catalysts, charge-transfer tran-

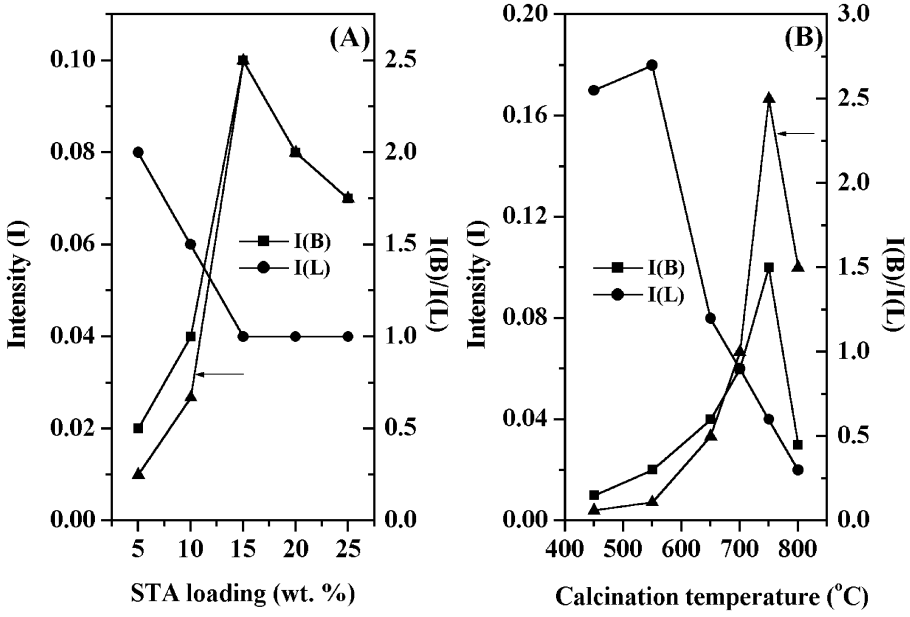

Fig. 8. Change in Brönsted acidity (B), Lewis acidity (L) and B/L ratio of (A) catalyst with different STA loading calcined at 750 °C and (B) 15 SZ calcined at different temperatures after in situ activation at 300 °C.

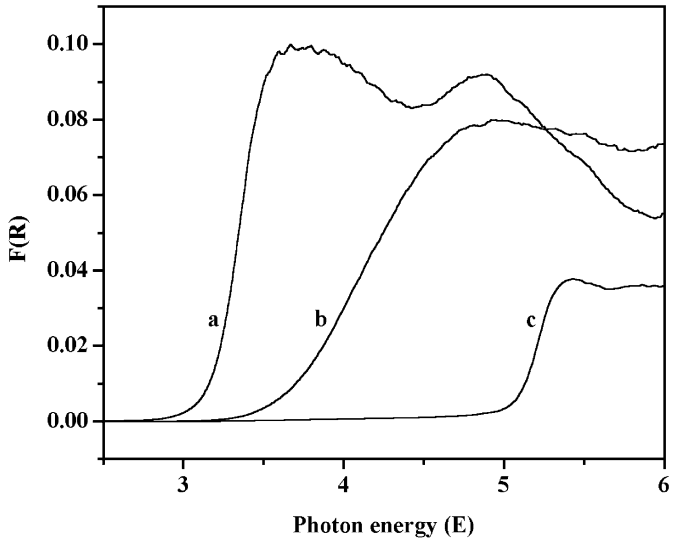

Fig. 9. DRUV–vis absorption spectra of (a) pure STA, (b) 15 SZ-750, (c) Z-750.

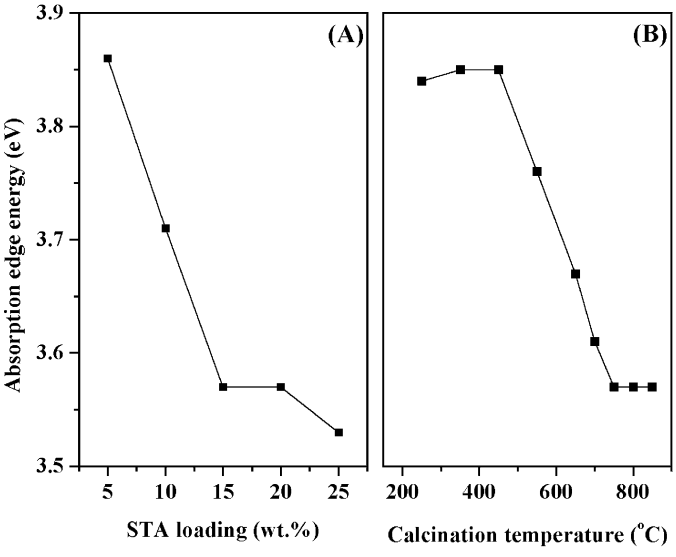

Fig. 10. Change in absorption edge energies of (A) catalyst with different STA loading calcined at 750 °C and (B) 15 SZ calcined at different temperatures.

sitions are more accurately characterized by the energy at the absorption edge. The fundamental optical absorption edge energies were determined using a procedure reported by Barton et al. [43] from the intercept of $[F(R)h\nu]^{1/2}$ plotted versus $h\nu$, where $F(R)$ is Kubelka–Munk function and $h\nu$ is the energy of the incident photon.

The absorption edge energies for the catalysts with different STA loadings calcined at 750 °C and for the catalyst 15 SZ calcined at different temperatures are shown in Fig. 10. Pure STA showed an absorption edge energy of 3.19 eV, whereas pure ZrO_2 showed an absorption edge energy of 5.04 eV. After supporting STA on zirconium oxyhydroxide (15%) followed by drying at 250 °C, the edge energy was increased to 3.84 eV. The increase in the edge energy compared with that of bulk STA was due to the effect of the support, which spread silicotungstate and thus decreased the interaction between the polyanions [44]. There was no appreciable change in edge energy for the catalyst

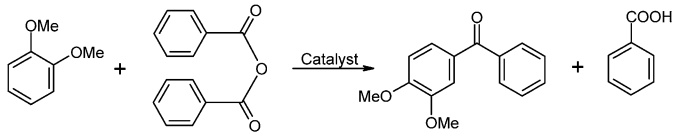

Scheme 1.

15 SZ up to a calcination temperature of 450 °C. A further increase in calcination temperature decreased the edge energy up to 750 °C. For catalysts with different STA loadings calcined at 750 °C, the edge energy decreased up to 15% loading. Edge energy did not change appreciably with further increases in STA loading. Thus the decrease in absorption edge energy with STA loading and calcination temperature up to a monolayer of silicotungstate on zirconia (15 SZ-750) could be explained on the basis of the interaction between polyanions. As the loading and calcination temperature increases, silicotungstate undergoes agglomeration, resulting in increased interaction between polyanions, which could be considered equivalent to the formation of a larger polyanion, resulting in decreased absorption edge energy [44,45].

The increase in Brönsted acidity with loading and calcination temperature can be explained on the basis of the interaction between polyanions and hence the formation of larger polyanion. Larger polyanions can effectively delocalize the negative charge required for the formation of Brönsted acid centers, ultimately resulting in increased Brönsted acidity.

The results from the various characterizations can be summarized as follows. The X-ray diffractograms of the catalysts with different STA loadings and calcination temperatures, along with Raman spectra of the catalyst 15 SZ, showed the presence of zirconia-anchored mono-oxotungstate as the major tungsten species up to an STA loading of ca. 15% at 750 °C. The results from other characterization techniques, such as NH_3-TPD and FTIR pyridine adsorption, indicated that catalyst 15 SZ-750 had the highest acidity. Characterization of the catalysts by XPS showed that a monolayer of silicotungstate on zirconia was attained for catalyst 15 SZ-750.

Consequently, we describe the evolution of the catalysts as follows. Up until a STA loading of ca. 15% at 750 °C, or for a 15% catalyst up to a calcination temperature of 750 °C (i.e., up to a monolayer), the surface of the catalyst was occupied mainly by mono-oxotungstate. Below this monolayer coverage, acidity of the catalyst increased with STA loading and calcination temperature. When the surface coverage exceeded monolayer, the formation of crystalline WO_3 occurred, accompanied by a decrease in Brönsted acidity.

3.2. Catalytic activity

The benzoylation of veratrole with benzoic anhydride over supported HPA catalysts led to the formation of 3,4-dimethoxy benzophenone as the benzoylated product (Scheme 1). This conversion was expressed as the percentage of BA converted into the product; the BA conversions on SZ catalysts with various STA loadings and calcination temperatures are shown in Fig. 11A. For catalysts with different STA loadings calcined at

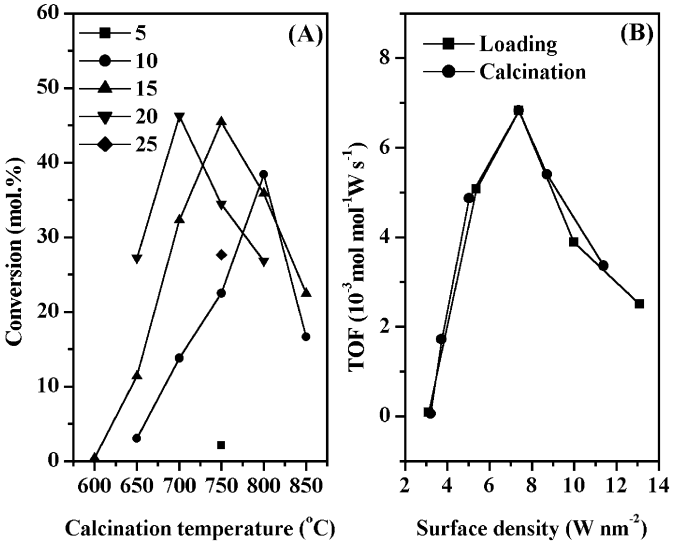

Fig. 11. Change in BA conversion with (A) STA loading and calcination temperature and (B) TOF versus surface density of catalysts with different STA loading calcined at 750 °C and 15 SZ calcined at different temperatures (conditions: temperature, 80 °C; total weight, 5 g; veratrole/BA (molar ratio) = 5; catalyst weight, 0.15 g; time, 1 h).

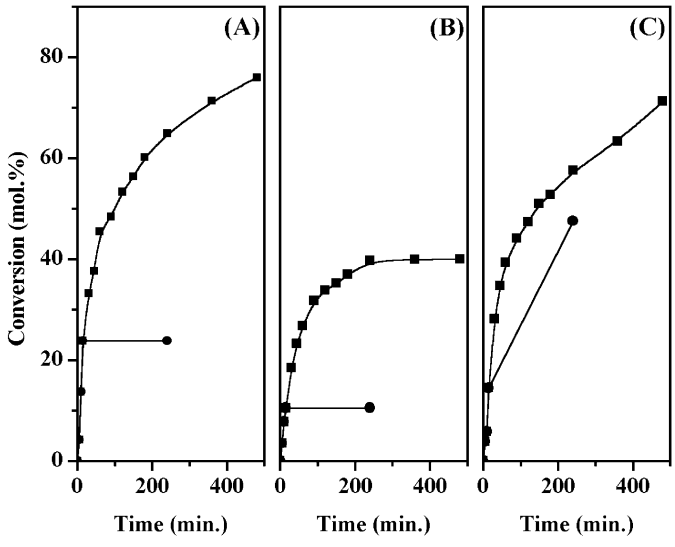

Fig. 12. Effect of time on BA conversion over the catalysts (A) 15 SZ-750, (B) 15 PZ-750, and (C) 15 SS-300, where ■ stands for reaction with fresh catalyst and ● reaction after catalyst separation by hot filtration (conditions: temperature, 80 °C; total weight, 5 g; veratrole/BA (molar ratio) = 5; catalyst weight, 0.15 g).

750 °C, BA conversion increased with loading, reaching a maximum at 15% STA and decreasing thereafter.

Interestingly, the BA conversion was found to depend strongly on catalyst calcination temperature. For instance, three catalyst samples with 10, 15, and 20% STA loading calcined at 600–850 °C, were used in the reaction (Fig. 11A). The sample with the highest STA loading (20%) showed maximum conversion at lower calcination temperature (700 °C), whereas the sample with the lowest STA loading (10%) showed the maximum conversion at higher calcination temperature (800 °C).

To establish the relation between catalytic activity, STA loading, and calcination temperature, the turnover frequency (TOF, mol $\text{mol}_{\text{W}}^{-1}$ s^{-1}) of catalysts with different STA loadings (5–25%) calcined at 750 °C and of 15 SZ calcined at 600–850 °C were determined (Fig. 11B). The catalyst 15 SZ-750 with a surface density of 7.4 W nm^{-2}, corresponding to monolayer coverage of STA on zirconia, gave the highest TOF in the reaction. This result explicitly shows that, irrespective of STA loading and calcination temperature, catalytic activity depends on STA coverage, and the highest activity corresponds to monolayer of STA on zirconia. It is also interesting to note that acidity measurements of the catalysts by FTIR pyridine adsorption and NH_3-TPD showed that the catalyst 15 SZ-750 had the highest total acidity as well as Brönsted acidity, clearly indicating that benzoylation of veratrole by benzoic anhydride was catalyzed by Brönsted acid sites present in the supported catalyst.

The activity of catalyst 15 SZ-750 was compared with that of the catalysts 15 PZ-750 and 15 SS-300 (Fig. 12). The catalysts 15 SZ-750 and 15 SS-300 exhibited similar reaction profiles, which differ from the reaction profile of 15 PZ-750. Because HPAs are soluble in polar solvents, it is important to study the heterogeneity of the catalysts in the reaction. For this, the reaction was stopped after 15 min, the catalyst was separated under hot conditions, and the hot filtrate was monitored for further reaction up to 4 h (Fig. 12). From Fig. 12, it is apparent that no change in BA conversion with time for filtrates was obtained from the catalysts 15 SZ-750 and 15 PZ-750; however, for the filtrate obtained from the catalyst 15 SS-300, the conversion increased from 14% after 15 min to 48% after 4 h. The analysis of the filtrate by ICP-OES showed that 70% STA from the catalyst 15 SS-300 leaches to the reaction medium during reaction. This clearly indicates that STA and PTA on zirconia acted as heterogeneous catalysts, whereas STA on silica was not stable and leached into the reaction medium during reaction.

Nonetheless, it is interesting to note that the heterogeneous catalysts 15 SZ-750 and 15 PZ-750 showed different catalytic behavior. For the catalyst 15 SZ-750, conversion of BA increased continuously with time and reached 76% after 480 min, whereas for the catalyst 15 PZ-750, a clear deactivation occurred, reaching a plateau between 240 and 480 min before reaching maximum conversion. This reaction profile, particularly with the catalyst 15 PZ-750, is similar to that reported for zeolite [2–4] and HPA [6–9] catalyzed acylation reactions, where the catalyst deactivation is attributed mainly to the strong adsorption of the acylation product on the catalyst, which blocks the accessibility of the reactants to the active sites. The kinetic profile of the reaction with catalysts 15 SZ-750 and 15 PZ-750 indicates that product inhibition was more prominent with 15 PZ-750 (Fig. 12).

In an attempt to explain the difference in the catalytic behavior, the catalyst 15 PZ-750 was characterized by different methods. The surface area, surface density (Table 1), XRD (not shown), and Raman spectrum of 15 PZ-750 were found to be similar to that of 15 SZ-750. The absorption edge energy of 15 PZ-750 (3.7 eV) was found to be slightly higher than that of 15 SZ-750 (3.57 eV). NH_3-TPD showed that 15 PZ-750 had a slightly higher acidity than 15 SZ-750 (Table 1). However,

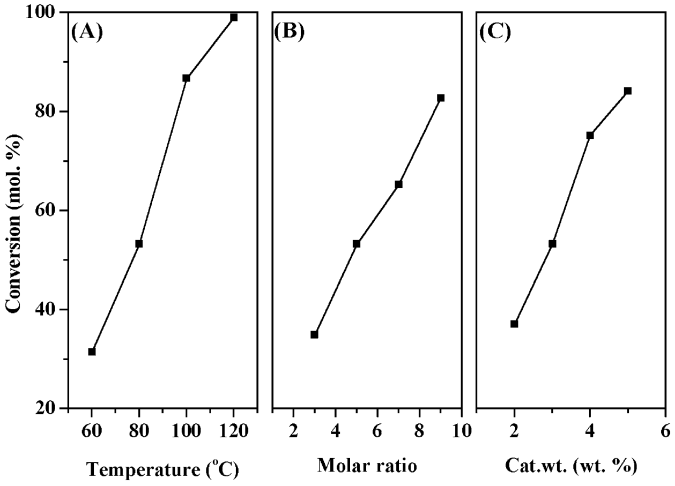

Fig. 13. Effect of reaction conditions on BA conversion. (A) Effect of temperature (conditions: total weight, 5 g; veratrole/BA (molar ratio) = 5; catalyst weight, 0.15 g; time, 2 h). (B) Effect of molar ratio (conditions: temperature, 80 °C; total weight, 5 g; catalyst weight, 0.15 g; time, 2 h). (C) Effect of catalyst weight (conditions: temperature, 80 °C; total weight, 5 g; veratrole/BA (molar ratio) = 5; time, 2 h).

FTIR pyridine adsorption studies revealed that the Lewis acidity was higher for 15 PZ-750 than for 15 SZ-750 (Table 2). Anderson et al. [9] have reported that catalysts with higher Lewis acidity are more susceptible to deactivation by product inhibition. Thus the higher conversion and greater deactivation resistance of the catalyst 15 SZ-750 is due to the greater number of strong Brönsted acid sites.

Therefore, the catalyst with the highest activity (15 SZ-750) was used to study different reaction parameters. The influence of temperature on BA conversion was studied in the temperature range 60–120 °C for 2 h (Fig. 13A). The conversion was 31% at 60 °C and it increased to 99% at 120 °C. The influence of veratrole/BA molar ratio (3–9) on BA conversion was studied, keeping the total weight of the reaction mixture constant (Fig. 13B). At a molar ratio of 3, the BA conversion was 35%, and as the molar ratio increased to 9, conversion increased to 83%. This was probably due to the inhibiting effect of 3,4-dimethoxy benzophenone, which can be strongly adsorbed on the catalyst surface. This inhibiting effect would be less significant for mixtures richer in veratrole, because the excess veratrole acts as a solvent for the ketone produced, thus reducing product inhibition, and therefore the BA conversion is higher at higher veratrole/BA molar ratios [4,46]. A catalyst concentration of 2 wt% (of the total mass of the reactants) gave a BA conversion of 37%, and a catalyst concentration of 5 wt% increased the BA conversion to 84% (Fig. 13C), due to the increase in the number of active sites of the catalyst.

For supported HPA catalysts, it is important to study recycling of the catalyst, because the limited thermal stability of HPAs usually prevents regeneration of the deactivated catalyst by thermal methods. To study recycling, the catalyst after reaction (120 °C, 3 wt% catalyst, 2 h, and a 5:1 molar reactant ratio) was separated, washed with dichloromethane, dried at 120 °C for 4 h, and reused with fresh reaction mixture. After the first use, the catalyst retained only 40% of the initial conversion.

Table 3
Benzoylation of veratrole with benzoic anhydride: the catalyst 15 SZ-750 versus zeolite H-Y[a]

Catalyst	Veratrole conversion (mol%)	TOF (mol $mol^{-1}_{H^+}$ h^{-1})
H-Y[b]	75	14
15 SZ-750	40	27

[a] Conditions: veratrole, 1.38 g (10 mmol); benzoic anhydride, 2.26 g (10 mmol); chlorobenzene, 50 ml; catalyst weight, 0.5 g; temperature, 130 °C; time, 1 h.
[b] Si/Al = 15.

The lower activity of the separated catalyst may be due to the presence of surface-bound benzoate species formed from the byproduct benzoic acid, which is difficult to remove by washing [9,47]. However, the catalytic activity was increased to 95% of the initial activity after regeneration of the catalyst by calcination at 500 °C for 4 h [27].

Table 3 compares the catalytic activity of 15 SZ-750 with those for H-Y zeolite under the reaction conditions reported elsewhere [5]. Catalyst TOFs were expressed as the number of moles of veratrole converted per mole of protons in the catalyst per hour (mol mol^{-1} h^{-1}). For zeolite H-Y (Si/Al = 15), the number of active protons was taken to be equivalent to the Al content [6], and for the catalyst 15 SZ-750, the number of protons was calculated from the nominal $H_4SiW_{12}O_{40}$ loading on ZrO_2 (calculated from the weight loss obtained in TG analysis) [29]. The zeolite H-Y exhibited greater veratrole conversion, but the catalyst 15 SZ-750 was more active and its TOF was nearly two times greater than that of H-Y.

4. Conclusions

The liquid-phase benzoylation of veratrole with benzoic anhydride was carried out over a series of zirconia-supported STA catalysts. The catalytic activity was found to depend mainly on the STA coverage, and the highest activity corresponded to a monolayer of silicotungstate on zirconia. A comparison of the catalytic activity of catalyst 15 SZ-750 with that of catalysts 15 PZ-750 and 15 SS-300 showed that zirconia-supported silicotungstic acid and phosphotungstic acid acted as efficient and stable solid acid catalysts, whereas silica-supported silicotungstic acid leached into the reaction medium and catalyzed the reaction homogeneously. Under the reaction conditions of 120 °C, a veratrole/BA molar ratio of 5, and 2 h, the most active catalyst, 15 SZ-750, gave 99% BA conversion, and the deactivated catalyst could be regenerated by calcination with no appreciable loss in activity.

Acknowledgments

This work was carried out with the support of a DST SERC project grant. BMD acknowledges CSIR New Delhi (India) for the award of a research associateship. The authors thank Dr. K.R. Patil for the XPS measurements and Dr. H.J. Goecke of the Institute for Inorganic and Analytical Chemistry, Munster, Germany for the Raman spectra measurements.

References

[1] G. Olah, Friedel–Crafts and Related Reactions, Wiley, New York, 1963–1964.
[2] D. Rohan, C. Canaff, E. Fromentin, M. Guisnet, J. Catal. 177 (1998) 296.
[3] E.G. Derouane, C.J. Dillon, D. Bethell, S.B. Derouane-Abd Hamid, J. Catal. 187 (1999) 209.
[4] E.G. Derouane, G. Crehan, C.J. Dillon, D. Bethell, H. He, S.B. Derouane-Abd Hamid, J. Catal. 194 (2000) 410.
[5] T. Raja, A.P. Singh, A.V. Ramaswamy, A. Finiels, P. Moreau, Appl. Catal. A 211 (2001) 31.
[6] J. Kaur, K. Griffin, B. Harrison, I.V. Kozhevnikov, J. Catal. 208 (2002) 448.
[7] I.V. Kozhevnikov, Appl. Catal. A 256 (2003) 3.
[8] L.A.M. Cardoso, W.A. Jr, A.R.E. Gonzaga, L.M.G. Aguiar, H.M.C. Andrade, J. Mol. Catal. A 209 (2004) 189.
[9] B. Bachiller-Baeza, J.A. Anderson, J. Catal. 228 (2004) 225.
[10] V. Quaschning, J. Deutsch, P. Druska, H.-J. Niclas, E. Kemnitz, J. Catal. 177 (1998) 164.
[11] K. Arata, H. Nakamura, M. Shouji, Appl. Catal. A 197 (2000) 213.
[12] J. Deutsch, H.A. Prescott, D. Müller, E. Kemnitz, H. Lieske, J. Catal. 231 (2005) 268.
[13] M.T. Pope, Heteropoly and Isopoly Oxometalates, Springer-Verlag, Berlin, 1983.
[14] T. Okuhara, N. Mizuno, M. Misono, Adv. Catal. 41 (1996) 113.
[15] C.L. Hill (Ed.), Chem. Rev. 98 (1998) 1.
[16] Y. Wu, X. Ye, X. Yang, X. Wang, W. Chu, Y. Hu, Ind. Eng. Chem. Res. 35 (1996) 2546.
[17] I.V. Kozhevnikov, Chem. Rev. 98 (1998) 171.
[18] K. Tanabe, T. Yamaguchi, Catal. Today 20 (1994) 185.
[19] G.K. Chuah, Catal. Today 49 (1999) 131.
[20] G.D. Yadav, J.J. Nair, Microporous Mesoporous Mater. 33 (1999) 1.
[21] S. Kuba, P. Lukinskas, R.K. Grasselli, B.C. Gates, H. Knözinger, J. Catal. 216 (2003) 353, and reference there in.
[22] E. Lopez-Salinas, J.G. Hermandez-Cortez, M.A. Cortes-Jacome, J. Navarrete, M.E. Llanos, A. Vazquez, H. Armendariz, T. Lopez, Appl. Catal. A 175 (1998) 43.
[23] E. Lopez-Salinas, J.G. Hermandez-Cortez, I. Schifter, E. Torres-Garcia, J. Navarrete, A. Gutierrez-Carrillo, T. Lopez, P.P. Lottici, D. Bersani, Appl. Catal. A 193 (2000) 215.
[24] S. Patel, N. Purohit, A. Patel, J. Mol. Catal. A 192 (2003) 195.
[25] B.M. Devassy, S.B. Halligudi, S.G. Hegde, A.B. Halgeri, F. Lefebvre, Chem. Commun. (2002) 1074.
[26] B.M. Devassy, F. Lefebvre, S.B. Halligudi, J. Catal. 231 (2005) 1.
[27] B.M. Devassy, G.V. Shanbhag, S.P. Mirajkar, W. Böhringer, J. Fletcher, S.B. Halligudi, J. Mol. Catal. A 233 (2005) 141.
[28] M.T. Echizen, K. Nagata, Y. Yoshinaga, T. Okuhara, J. Mol. Catal. A 201 (2003) 145.
[29] D.G. Barton, S.L. Soled, G.D. Meitzner, G.A. Fuentes, E. Iglesia, J. Catal. 181 (1999) 57.
[30] JCPDS-International Center for diffraction data, 1990, Card 43-1035.
[31] C. Rocchiccioli-Deltcheff, M. Fournier, R. Franck, R. Thouvenot, Inorg. Chem. 22 (1983) 207.
[32] C.M. Teague, X. Li, M.E. Biggin, L. Lee, J. Kim, A.A. Gewirth, J. Phys. Chem. B 108 (2004) 1974.
[33] S. Loridant, C. Feche, N. Essayem, F. Figueras, J. Phys. Chem. B 109 (2005) 5631.
[34] M. Scheithauer, R.K. Grasselli, H. Knözinger, Langmuir 14 (1998) 3019.
[35] I.V. Kozhevnikov, in: Catalysis by Polyoxometalates, Catalysts for Fine Chemical Synthesis, vol. 2, Wiley, New York, 2002, p. 15.
[36] M. Valigi, D. Gazzoli, G. Ferraris, E. Bemporad, Phys. Chem. Chem. Phys. 5 (2003) 4974.
[37] M. Valigi, D. Gazzoli, I. Pettiti, G. Mattei, S. Colonna, S.D. Rossi, G. Ferraris, Appl. Catal. A 231 (2002) 159.
[38] F.J. Gil-Llambías, A.M. Escudey, J.L.G. Fierro, A.L. Agudo, J. Catal. 95 (1985) 520.
[39] M.S. Kaba, I.K. Song, D.C. Duncan, C.L. Hill, M.A. Barteau, Inorg. Chem. 37 (1998) 398.
[40] G. Busca, Catal. Today 41 (1998) 191.
[41] B.H. Davis, R.A. Keogh, S. Alerasool, D.J. Zalewski, D.E. Day, P.K. Doolin, J. Catal. 183 (1999) 45.
[42] A. Khodakov, J. Yang, S. Su, E. Iglesia, A.T. Bell, J. Catal. 177 (1998) 343.
[43] D.G. Barton, M. Shtein, R.D. Wilson, S.L. Soled, E. Iglesia, J. Phys. Chem. B 103 (1999) 630.
[44] M. Fournier, C. Louis, M. Che, P. Chaquin, D. Masure, J. Catal. 119 (1989) 400.
[45] D. Masure, P. Chaquin, C. Louis, M. Che, M. Fournier, J. Catal. 119 (1989) 415.
[46] P. Botella, A. Corma, J.M. López-Nieto, S. Valencia, R. Jacquot, J. Catal. 195 (2000) 161.
[47] A. Trunschke, J. Deutsch, D. Müller, H. Lieske, V. Quaschning, E. Kemnitz, Catal. Lett. 83 (2002) 271.